POLITECNICO DI TORINO
Repository ISTITUZIONALE

Reticular chemistry for the rational design of mechanically robust mesoporous merged-net metal-organic frameworks

(Article begins on next page)

08 May 2024

Matter

Article

Reticular chemistry for the rational design of mechanically robust mesoporous merged-net metal-organic frameworks
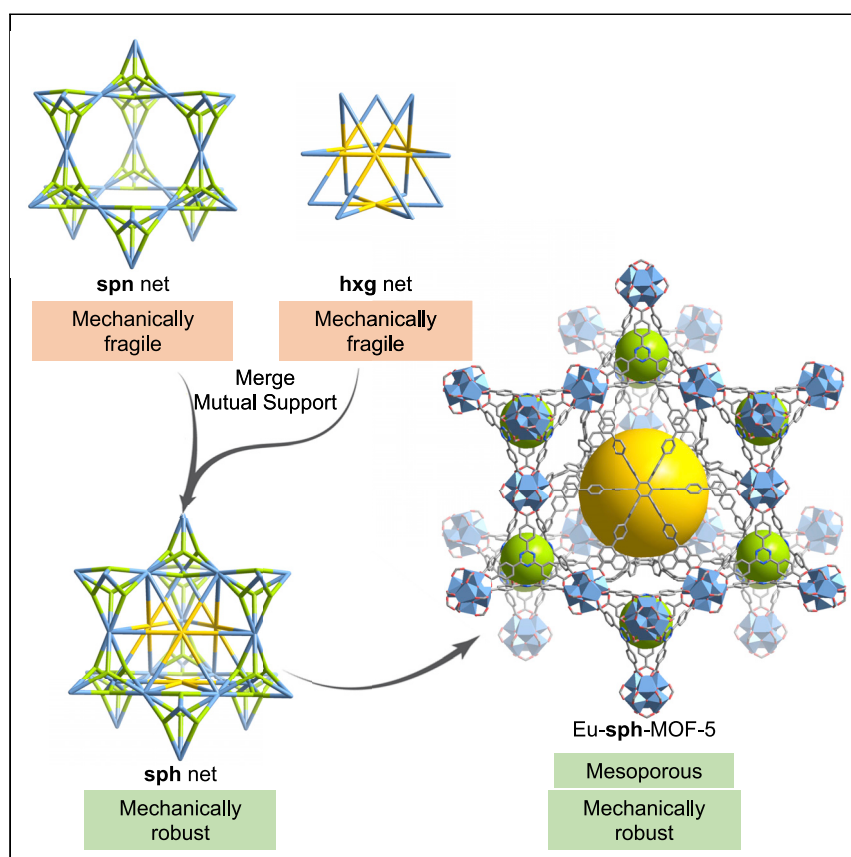
Mechanical stability plays a key role in the practical applications of metal-organic frameworks (MOFs). This study provides new insight into the design of high-mechanical-stability MOFs by merging two mechanically fragile frameworks into a more robust framework. A mesoporous MOF with high mechanical stability was synthesized by combining the topological merged-net approach and the introduction of triangular rigidity. The enhancement of mechanical stability was studied by computational force field calculation and experimental AFM characterization.

3 **Understanding**
Dependency and conditional studies on material behavior

Hao Jiang, Seyed Mohamad Moosavi, Justyna Czaban-Jóźwiak, ..., Enzo Di Fabrizio, Berend Smit, Mohamed Eddaoudi

berend.smit@epfl.ch (B.S.)
mohamed.eddaoudi@kaust.edu.sa (M.E.)

Highlights

Reveal mechanical enhancement of merged frameworks in reticular chemistry

Computational calculation of three mechanisms impacts MOFs' mechanical stability

Synthesis of a high-mechanical-stability mesoporous mixed-linker MOF, RE-**sph**-MOF-5

AFM mechanical stability study of synthesized **sph**-MOFs

Article

Reticular chemistry for the rational design of mechanically robust mesoporous merged-net metal-organic frameworks

Hao Jiang,[1,6] Seyed Mohamad Moosavi,[2,6] Justyna Czaban-Jóźwiak,[1] Bruno Torre,[3,4]
Aleksander Shkurenko,[1] Zied Ouled Ameur,[1] Jiangtao Jia,[1] Norah Alsadun,[1,5] Osama Shekhah,[1]
Enzo Di Fabrizio,[3,4] Berend Smit,[2,*] and Mohamed Eddaoudi[1,7,*]

SUMMARY

Access to metal-organic frameworks (MOFs) with enhanced mechanical stability is key to their successful deployment in practical applications. However, the high porosity of the material often affects mechanical stability. In this article, to achieve highly porous MOFs with enhanced mechanical stability, we explored the merged-net approach where two relatively fragile frameworks were merged into a robust MOF structure. We demonstrate the effectiveness of this approach by computationally evaluating mechanical properties of sph-MOFs with varying lengths of linkers. Prominently, we pinpoint the significance of triangular rigidity on the robustness of large-pore MOFs and, subsequently, designed and synthesized a rare earth (RE)-based RE-sph-MOF-5 by the reticulation of hexanuclear RE clusters, tritopic linkers, and unprecedentedly large planar hexatopic linkers containing 19 phenyl rings. The mechanical properties of sph-MOFs were characterized and quantified using amplitude-frequency modulation (AM-FM) bimodal atomic force microscopy (AFM) analyses. Markedly, the mesoporous RE-sph-MOF-5 expresses high mechanical stability despite its large mesoporous cavities.

INTRODUCTION

Metal-organic frameworks (MOFs) are a class of crystalline porous materials comprised of periodically linked inorganic metal ions/clusters and organic ligands.[1,2] The successful deployment of the reticular chemistry based on various building-block approaches paved the way for the deliberate construction of myriad porous materials with remarkable properties.[3,4] The ability of structural control and modification provides MOFs capable of a wide range of intriguing applications such as gas storage and separation,[5–9] catalysis,[10–12] electrochemical reduction,[13,14] and energy storage.[15]

Markedly, prospect applications of MOFs (e.g., hydrocarbon separations, high-pressure gas storage, catalysis, etc.) depend on MOF-associated stabilities.[16–19] In contrast to chemical stability and thermal stability, mechanical stability remains less explored.[16,18,20,21] Advances in calculation/prediction methods[22–27] and various specialized characterization techniques such as nanoindentation[28,29] and atomic force microscopy (AFM) nanoindentation[30] offer the potential to study and evaluate mechanical properties of extended solid-state materials, such as MOFs. Recently, the

PROGRESS AND POTENTIAL

The linker expansion, affording extra-large, free open space in metal-organic frameworks (MOFs), is generally accompanied by a decrease in their mechanical stabilities, which makes it difficult to obtain highly stable mesoporous MOFs with elongated linkers. Here, we demonstrate the combination of the merged-net approach and triangular rigidity as an effective strategy for the rational design of mechanically robust mesoporous MOFs. The merged-net approach can merge two mechanically fragile frameworks into a more robust framework, and the introduction of rigid triangular structures can further increase their mechanical stability. We report RE-sph-MOF-5 as an example containing both high porosity and high mechanical stability without losing much porosity. We expect this work will further promote the synthesis of mechanically robust materials, i.e., MOFs and COFs, as various other potential merged nets offer great potential for the synthesis of mechanically stable structures.

enhancement of mechanical stability for MOFs attracted more attention, and some post-modification methods such as ligand retrofitting,[31] covalent cross-linking,[32] and polymer insertion[33] have been reported to increase the stability of mechanically fragile MOFs. However, the direct topological design method of mechanically robust, highly porous MOFs remains less explored.[16,31]

Reticular chemistry is widely used for the prediction and design of diverse types of periodic extended structures.[2,3,34,35] During the past two decades of exploration, edge-transitive nets, nets with one type of edge, were found to be ideal targets of simple structures in reticular chemistry.[2,36,37] Recently, we introduced a systematic design principle, named the merged-net strategy, targeting the design of more complex mixed-linker MOFs.[38] The merge of two edge-transitive nets, (3,6)-c **spn** net (transitivity [21]) and 6-c **hxg** net (transitivity [11]), will lead to a merged minimal edge-transitive net,[36,39] (3,6,12)-c **sph** net (transitivity [32]), with a relatively higher complexity (Figure S1). The merged **sph** net inherited the structural properties from both parent nets and encompassed the ability to be an ideal design target in reticular chemistry. Based on the **sph** net, two frameworks can merge through shared inorganic molecular building blocks (MBBs), thus leading to the effective design of intricate mixed-linker MOFs. Practically, utilizing the merged-net approach, we synthesized a series of highly symmetric mixed-linker MOFs, named **sph**-MOF-1 to -4, based on the 12-c hexanuclear rare earth (RE) clusters.[38]

Here, we show the merged-net approach as an effective method to design mechanically robust and highly porous MOFs. In the merged-net MOFs, the two 3-periodic frameworks are mutually supporting each other, which gives another 3-periodic structure with enhanced mechanical stability without much loss of pore access. This phenomenon results in merged MOFs with increased mechanical stability. Although both **spn** and **hxg** nets are mechanically fragile nets, the merged **sph** nets are mechanically robust because of the mutual mechanical support of both parent nets. The improvement observed in the mechanical stability of merged-net MOFs set these materials among the MOFs with the highest mechanical stability based on the same size of ligand. Markedly, we report the design and synthesis of Eu-**sph**-MOF-5 as an example of materials owning both mesoporosity and high mechanical stability.

RESULTS

Merged nets and sph-MOF-1 to -4

Our previous reported RE-**sph**-MOFs (**sph**-MOF-1 to -4) represent the first systematically studied merge-net platform.[38] All the structures are mixed-linker frameworks based on merged-net **sph**. These MOFs contain hexanuclear RE clusters, smaller tritopic linkers for **spn** frameworks, and larger hexatopic linkers (or two tritopic linkers) for **hxg** frameworks. By removing the smaller tritopic linker, it will be only the **hxg** part left, while by removing the larger hexatopic linkers, it will be only the **spn** part left (Figure 1).

Concretely, all the **sph**-MOFs are based on an RE hexanuclear cluster (Figure 1A) and contain two types of organic linkers (Figure 1B). The small-size **sph**-MOF-1 contains 5-(4H-1,2,4-triazol-4-yl)isophthalate (TIA) for the **spn** part and 4,4′,4″-((benzene-1,3,5-tricarbonyl)tris(azanediyl))tribenzoate (BTCB) for the **hxg** part. The medium-size **sph**-MOF-2 contains benzotristhiophene carboxylate (BTTC) for the **spn** part and 4,4′,4″-(benzene-1,3,5-triyltris-(benzene-4,1-diyl))tribenzoate (BTPB) for the **hxg** part. The **sph**-MOF-3 contains the same BTTC linker as **sph**-MOF-2 for the **spn** part but hexacarboxylate ligand, hexakis(4-(4-carboxyphenyl)phenyl)

[1]Functional Materials Design, Discovery and Development Research Group (FMD[3]), Advanced Membranes and Porous Materials Center (AMPMC), Division of Physical Sciences and Engineering (PSE), King Abdullah University of Science and Technology (KAUST), Thuwal 23955-6900, Kingdom of Saudi Arabia

[2]Laboratory of Molecular Simulation, Institut des Sciences et Ingénierie Chimiques, École Polytechnique Fédérale de Lausanne (EPFL), Rue de l'Industrie 17, 1951 Sion, Valais, Switzerland

[3]SMILEs Lab, Physical Science and Engineering (PSE) and Biological and Environmental Science and Engineering (BESE) Divisions, King Abdullah University of Science and Technology, Thuwal 23955-6900, Kingdom of Saudi Arabia

[4]DISAT Department, Politecnico di Torino, Corso Duca degli Abruzzi 24, 10129 Torino, Italy

[5]Department of Chemistry, College of Science, King Faisal University (KFU), Al-Ahsa 31982-400, Kingdom of Saudi Arabia

[6]These authors contributed equally

[7]Lead contact

*Correspondence: berend.smit@epfl.ch (B.S.), mohamed.eddaoudi@kaust.edu.sa (M.E.)
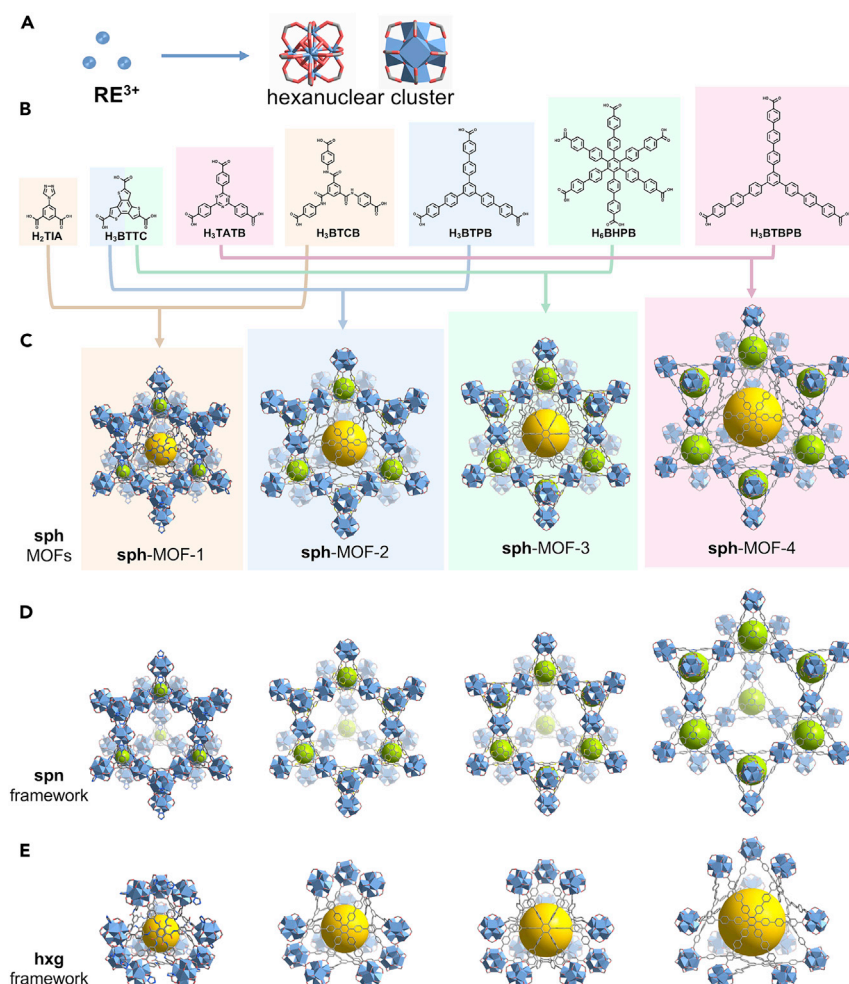
Figure 1. Schematic showing the structures of sph-MOFs used in this work for mechanical properties calculation

(A) Hexanuclear rare-earth clusters in **sph**-MOFs.

(B) Organic linkers used for the construction of **sph**-MOFs-1 to -4.

(C) Crystal structures of **sph**-MOFs-1 to -4. The background colors represent different MOFs: yellow for **sph**-MOF-1, blue for **sph**-MOF-2, green for **sph**-MOF-3, and pink for **sph**-MOF-4.

(D) The **spn** parts in corresponding **sph**-MOFs.

(E) The **hxg** parts in corresponding **sph**-MOFs.

benzoate (BHPB) (Figure S2) for the **hxg** part. The large-size **sph**-MOF-4 contains 4,4',4''-s-triazine-2,4,6-triyltribenzoate (TATB) for the **spn** part and 4,4',4''-(benzene-1,3,5-triyltris(biphenyl-4,4'-diyl))tribenzoate (BTBPB) for the **hxg** part (Figures 1C–1E). In the structures of sph-MOF-1, -2, and -4, the 6-c building blocks are constructed by two tritopic linkers in a staggered stacking mode (Figure S5).

Principles for enhancing mechanical stability of MOFs

We use a classical force field to compute the stiffness matrix for **sph**-MOFs since no breaking/formation of chemical bonds, nor other quantum effects, are involved in this study (see experimental procedures for details). In our previous work, we showed that these force fields provide sufficient accuracy in predicting the mechanical properties of MOFs.[22,40] For each **sph**-MOF, we use bulk, Young's, and shear moduli to characterize the mechanical stability. In Figure 2, we show these metrics for the MOFs (**sph**-MOF-1 to -4) and their corresponding **spn/hxg** parts.
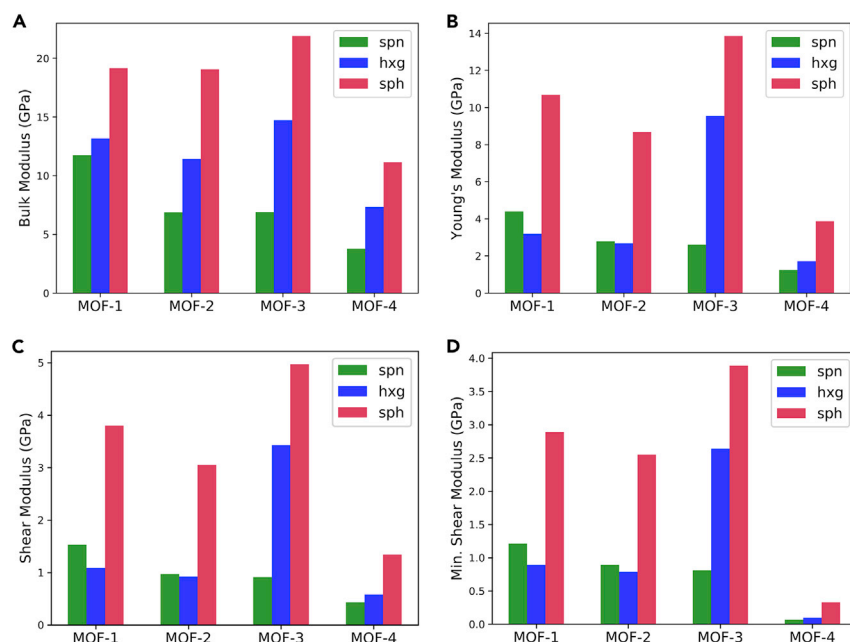
Figure 2. Comparison of force-field-calculated mechanical properties for sph-MOFs and the corresponding spn and hxg frameworks

(A–D) Bulk modulus (A), Young's modulus (B), shear modulus (C), and min. shear modulus (D) of **sph**-MOFs. The colors represent different parts of **sph**-MOFs: green only considers **spn** frameworks, blue only considers **hxg** frameworks, and red only considers whole **sph** frameworks.

We found three mechanisms for the design of MOFs with higher stability: (1) topologies (nets), (2) size and flexibility of linkers, and (3) triangular rigidity.

The first mechanism is the underlying topology, and the merged-net process shows significant enhancement to the parent-net frameworks. For all the **sph**-MOFs, the mechanical stabilities of merged **sph** frameworks are significantly higher compared with the corresponding **spn** and **hxg** frameworks, especially for Young's modulus and shear modulus (Figures 2B and 2C). With **sph**-MOF-2 as an example, the computed Young's modulus increased from 2.8 (**spn** framework) and 2.7 (**hxg** framework) to 8.7 GPa (**sph**-MOF-2), which are 211% and 222% increases, respectively. The computed shear modulus increased from 1.0 (**spn** framework) and 0.9 (**hxg** framework) to 3.1 GPa (**sph**-MOF-2), which are 210% and 244% increases, respectively. As a comparison, the theoretical pore volume by volume of **sph**-MOF-2 is only decreased by 21.4% for the **spn** framework and 9.2% for the **hxg** framework. The increment of mechanical stability of merged nets can be attributed to two aspects. First, the merging process results in nets of higher vertex coordinates, which means that the building blocks in merged-net structures have higher connectivity than those in the parent-net frameworks. Second, compared with each parent-net framework, the added organic linkers provide extra mechanical support to the other framework.

The second mechanism is the size and flexibility of linkers. As expected, we observed a decrease in the mechanical stability by expanding the ligands, e.g., comparing **sph**-MOF-1 with **sph**-MOF-2 and **sph**-MOF-4. All these MOFs contain two tritopic linkers. Indeed, among these three MOFs, **sph**-MOF-1, with the shortest ligands, has the highest mechanical stability, and **sph**-MOF-4, with the largest ligands, has the lowest mechanical stability. Relatively, the stability decrease of **sph**-MOF-2 is
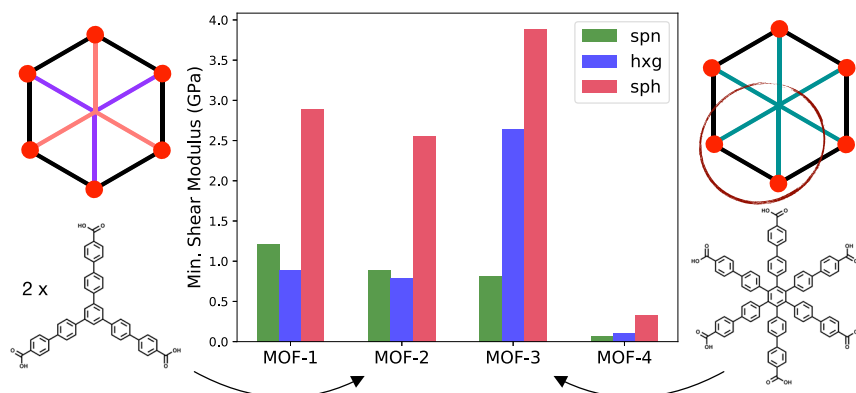
Figure 3. Schematic showing the triangle rigidity of sph-MOF-3
The high minimum shear modulus in **sph**-MOF-3 is associated with rigid triangles.

quite small compared with **sph**-MOF-1. Especially, the bulk moduli of **sph**-MOF-1 and **sph**-MOF-2 are almost the same (Figure 2A), which can be attributed to the slight flexibility of the amide group in the linker of **sph**-MOF-1.

The third mechanism is the triangular rigidity, allowing **sph**-MOF-3 to stand out from this trend (Figure 3, where we observe a 50% increase of minimum (min.) shear modulus from **sph**-MOF-2 to **sph**-MOF-3). The highly connected H_6BHPB ligands of **sph**-MOF-3 make a very strong network with enhanced mechanical stability in contrast to all the other evaluated structures in this study. We can infer the stability of this material to the triangle rigidity. Triangles are used widely in civil and mechanical engineering for construction structures (trusses in roofs, bridges, etc.) due to their high rigidity. The angles of a triangle cannot be deformed unless the edges change length. Therefore, the deforming/shearing MOF-3 is much more difficult as it requires expansion/compression of chemical bonds, in contrast to the angle deformation in the other frameworks.

An interesting prediction is to synthesize a new **sph**-MOF (**sph**-MOF-5) with the same type of triangular connectivity as **sph**-MOF-3 and the same large linker size as **sph**-MOF-4 (Figure S6). As **sph**-MOF-4 is relatively unstable, we expect that this modification would afford a material adapted to higher pressures.

Design and synthesis of mechanically robust mesoporous RE-sph-MOF-5

To increase the mechanical stability of mesoporous **sph**-MOFs, we designed our **sph**-MOF-5 with hexakis(4''-[1,1':4',1''-terphenyl]-4-carboxylate)benzene (BHBPB) ligand as the **hxg** linker (Figures 4A, S3, and S4). As far as we know, this is the first time that the H_6BHBPB compound was reported, and the linker contains 19 benzene rings, which is the highest number among all planar MOF linkers. **sph**-MOF-5 was designed with the same merged-net approach as other **sph**-MOFs. The calculated shear modulus of **sph**-MOF-5 is a 90% increase compared with the same-size framework **sph**-MOF-4.

Solvothermal reactions of $Eu(NO_3)_3 \cdot 5H_2O$, H_3TATB, and H_6BHBPB in a N,N-diethyl-formamide (DEF) solution in the presence of 2-fluorobenzoic acid (2-FBA) for 48 h at 115°C yielded colorless octahedral single crystals of **sph**-MOF-5. Single-crystal X-ray diffraction (SCXRD) studies revealed that **sph**-MOF-5 crystallized in the cubic space group Fd-3m with a unit cell parameter a = 57.439(1) (Figure 4B; Table S1). The compound formulated as $[(CH_3)_2NH_2]_2[Eu_6(\mu_3\text{-}OH)_8(TATB)_2(BHBPB)(H_2O)_3] \cdot x$(solv). The experimental powder X-ray diffraction (PXRD) pattern of as-synthesized and
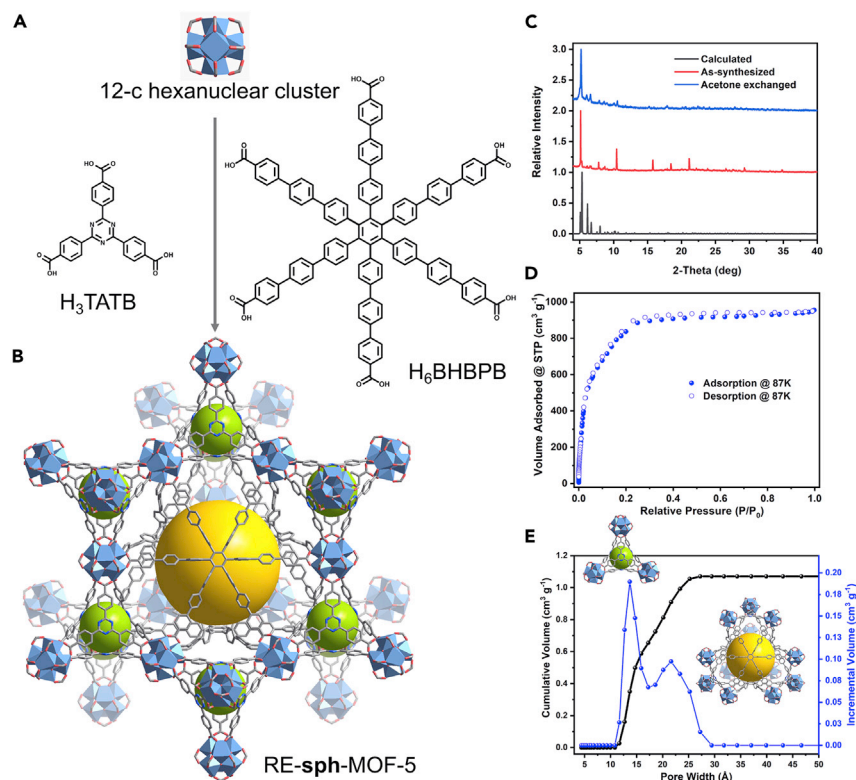
Figure 4. Schematic showing the structure and porosity of sph-MOF-5

(A) Hexanuclear rare earth cluster in Eu-**sph**-MOF-5 and two organic linkers used for the synthesis of Eu-**sph**-MOF-5.

(B) Structure of Eu-**sph**-MOF-5. The color balls represent different cages: yellow balls for large truncated tetrahedral cages, and green balls for small tetrahedral cages.

(C) PXRD pattern of calculated, as-synthesized, and acetone-exchanged Eu-**sph**-MOF-5.

(D) Ar adsorption isotherm at 87 K.

(E) Pore-size distribution calculated from Ar adsorption at 87 K.

acetone-exchanged Eu-**sph**-MOF-5 matches the calculated PXRD pattern derived from the SCXRD data (Figure 4C).

The topological analysis of **sph**-MOF-5 revealed that the 12-c hexanuclear Europium clusters are linked to the 3-c TATB linkers and the 6-c BHBPB linkers to form a 3-periodic MOF based on the underlying (3,6,12)-c **sph** net. The carbon atoms of the center triazine in the TATB linker can be regarded as points of extension of the 3-c nodes. The carbon atoms of the center benzene in the BHBPB linker can be regarded as points of extension of the 6-c nodes. The carbon atoms of the coordinated carboxylates can be presented as points of extension of the 12-c nodes.

The unique **sph** net and large organic linkers provide both microporous and mesoporous cages in the structure of **sph**-MOF-5. The larger truncated tetrahedral cages, having diameters of about 22 Å, are delimited by four BHBPB and four TATB linkers, while the smaller tetrahedral cages, having diameters of about 13 Å, are enclosed by four TATB linkers.

The activation of **sph**-MOF-5 was done by solvent exchange of acetone, followed by vacuum at 105°C. The permanent porosity of **sph**-MOF-5 has been examined by an argon-adsorption experiment at 87 K. The uptake of argon (Ar) at $P/P_0 = 0.95$ is

Table 1. Calculated mechanical properities of sph-MOFs and the corresponding spn/hxg frameworks

Structure	Bulk modulus (GPa)	Young's modulus (GPa)	Shear modulus (GPa)	Max. Young's modulus (GPa)	Min. Young's modulus (GPa)	Max. shear modulus (GPa)	Min. shear modulus (GPa)
MOF-1 spn	11.7	4.4	1.5	5.2	3.7	1.7	1.2
MOF-1 hxg	13.2	3.2	1.1	3.6	2.7	1.2	0.9
MOF-1 sph	19.2	10.7	3.8	19.6	8.6	5.8	2.9
MOF-2 spn	6.9	2.8	1.0	3.0	2.6	1.0	0.9
MOF-2 hxg	11.4	2.7	0.9	3.0	2.3	1.0	0.8
MOF-2 sph	19.1	8.7	3.1	11.1	7.3	3.9	2.6
MOF-3 spn	6.9	2.6	0.9	2.8	2.3	1.0	0.8
MOF-3 hxg	14.7	9.6	3.4	13.5	7.5	5.0	2.6
MOF-3 sph	21.9	13.9	5.0	19.3	11.0	7.1	3.9
MOF-4 spn	3.8	1.3	0.4	2.2	0.3	1.9	0.1
MOF-4 hxg	7.3	1.7	0.6	3.5	0.4	2.5	0.1
MOF-4 sph	11.1	3.9	1.3	8.1	1.2	4.7	0.3
MOF-5 spn	5.6	1.2	0.4	1.6	0.8	0.6	0.3
MOF-5 hxg	8.7	5.8	2.1	8.4	4.5	3.1	1.6
MOF-5 sph	14.5	7.7	2.7	10.3	6.4	3.7	2.2

about 940 cm^3 g^{-1} (Figure 4D). The apparent Brunauer-Emmett-Teller (BET) surface area was estimated to be 2,965 m^2 g^{-1}. The experimental total pore volume was estimated to be 1.21 cm$^3 \cdot$g^{-1} (at P/P$_0$ = 0.95), which is consistent with the theoretical pore volume of 1.29 cm$^3 \cdot$g^{-1}, based on the associated crystal structure. An increase at P/P$_0$ = 0.17 on the Ar adsorption isotherm corresponds to a mesoporous cage with a diameter of about 2.2 nm in **sph**-MOF-5 (Figure 4E).

The calculated mechanical properties of **sph**-MOF-5 are shown and compared with the other MOFs in Table 1. The bulk modulus, Young's modulus, and shear modulus of the **spn** part and the **hxg** part frameworks are 5.6, 1.2, and 0.4 and 8.7, 5.8, and 2.1 GPa, respectively. While the merged structure of **sph**-MOF-5 results in 14.5, 7.7, and 2.7 GPa, corresponding to 159%, 542%, and 575% increases, in contrast to the associated **spn** framework, and 66%, 33%, and 29% increases, in contrast to the associated **hxg** framework. Compared with **sph**-MOF-4, **sph**-MOF-5 has a similar pore size and pore volume, while the bulk modulus, Young's modulus, and shear modulus of **sph**-MOF-5 are increased from 11.1, 3.9, and 1.3 to 14.5, 7.7, and 2.7 GPa, corresponding to 30%, 97%, and 108% increases. The anticipated increase in mechanical stability is mainly attributed to the triangular windows contracted by 6-c linkers in **sph**-MOF-5.

Mechanical characterization of RE-sph-MOFs by amplitude-frequency modulation (AM-FM) bimodal AFM

To further confirm the conclusions obtained from the theoretical calculations, we characterized Young's modulus of microporous Eu-**sph**-MOF-3, mesoporous Eu-**sph**-MOF-4, and mesoporous Eu-**sph**-MOF-5 with the AF-FM mode of AFM (Figures 5 and S6). The tested crystals are in an octahedral shape with crystal diameters ranging from 100 to 200 μm (Figure S7). All characterizations are based on at least 512 × 512 tests on the triangle surface of crystals.

The Young's modulus of **sph**-MOF-4 ranges from 1 to 6 GPa with an average value of 3.7 GPa (Figure 5B), and the Young's modulus of **sph**-MOF-5 ranges from 3 to 12 GPa with an average value 7.8 GPa (Figure 5C). As expected, the mechanical stability of **sph**-MOF-5 is enhanced compared with **sph**-MOF-4, although they contain similar pore environments and structure sizes. The enhancement is contributed to the hexatopic BHBPB linker, which gives triangles rather than parallelograms in the structure (Figure S6).
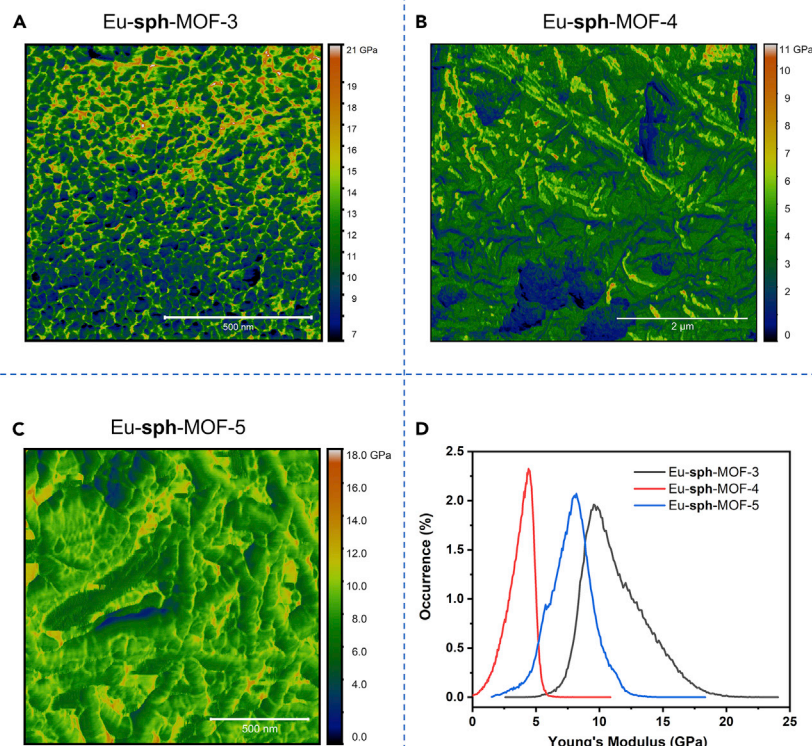
Figure 5. Bimodal AFM mechanical properties characterization of sph-MOFs

(A–C) Young's modulus for Eu-**sph**-MOF-3 (A), Eu-**sph**-MOF-4 (B), and Eu-**sph**-MOF-5 (C).

(D) Range of Young's modulus for Eu-**sph**-MOF-3 to -5.

The comparison of Young's moduli between **sph**-MOF-3 and **sph**-MOF-5 shows the impact of sizes on the mechanical stabilities of **sph** platforms. The characterized Young's modulus of **sph**-MOF-3 ranges from 7 to 18 GPa with an average value of 11.3 GPa (Figure 5A). Both **sph**-MOF-3 and **sph**-MOF-5 contain triangle rigidity, resulting in a much higher Young's modulus compared with **sph**-MOF-4 (Figure 5D). The characterized Young's modulus of **sph**-MOF-3 is 1.45 times that of **sph**-MOF-5 (11.3 versus 7.8 GPa), and the experimental pore volume of **sph**-MOF-5 is 1.68 times the pore volume of **sph**-MOF-3 (0.72 $cm^3 \cdot g^{-1}$ versus 1.21 $cm^3 \cdot g^{-1}$), which indicates that a balance of pore volume and mechanical stability should be considered in the utilization of MOFs.

DISCUSSION

We have explored the mechanical stability principle in merged-net materials based on isoreticular RE-**sph**-MOFs. The results show that the combination of the merged-net approach and triangular rigidity is an effective strategy to attain high porosity and high stability material mutually. The successful design and synthesis of mechanically robust mesoporous Eu-**sph**-MOF-5 demonstrate the effectiveness of this strategy. This work signifies that the merged-net approach offers great potential for the design and synthesis of highly stable porous materials, which will accelerate the discovery of functional materials for catalysis and energy storage. Markedly, this study paves the way to systematically study all the potential merged nets and their associated mechanical stability.

EXPERIMENTAL PROCEDURES

Resource availability

Lead contact

Further information and reasonable requests for resources and reagents should be directed to and will be fulfilled by the lead contact, Mohamed Eddaoudi (mohamed.eddaoudi@kaust.edu.sa).

Materials availability

The target materials can be synthesized following the procedures under experimental procedures and data in the supplemental information.

Data and code availability

Single-crystal structures of RE-**sph**-MOF-5 reported in this paper have been deposited at the Cambridge Crystallographic Data Center (CCDC). The accession number for the crystal structures is CCDC: 2174677. The data can be obtained free of charge from the CCDC via www.ccdc.cam.ac.uk/data_request/cif. All the necessary data have been presented in the main text and supplemental information. This study did not generate code.

Synthesis of Eu-sph-MOF-3 and Eu-sph-MOF-4

Eu-**sph**-MOF-3 and Eu-**sph**-MOF-4 were synthesized by a modified condition of our reported procedure.[38] Detailed synthesis conditions can be found in the supplemental information.

Synthesis of Eu-sph-MOF-5

$Eu(NO_3)_3 \cdot 5H_2O$ (18.7 mg), H_3TATB (5.3 mg), H_6BHBPB (10.1 mg), 2-FBA (400 mg), and DEF (6 mL) were combined and sonicated for 10 min. The solution was evenly distributed to four 20 mL scintillation vials. Extra 2-FBA (100 mg) was added to each vial. The vials were sealed, kept in a preheated oven at 115°C for 2 days, and cooled to room temperature. The colorless polyhedral crystals were collected and washed with DMF.

Calculations of the mechanical properties

The moduli of elasticity, including bulk, shear, and Young's moduli, are extracted from the stiffness matrix. We follow the same procedure of our previous work to compute the stiffness matrix, and we use a classical force field (Dreiding)[40] by fixing the metal geometry to the experimental crystal structure as implemented in the large-scale atomic/molecular massively parallel simulator (LAMMPS) interface.[41] In our previous work, we showed that these force fields provide sufficient accuracy in predicting the mechanical properties of MOFs.[22,41] All calculations were carried out within the LAMMPS molecular simulation package.[42]

To obtain the input files of the materials, we start with the single-crystal structure of RE-**sph**-MOFs. All the structures were prepared based on our published CIF files of **sph**-MOFs by manually removing solvent molecules and disorders.[36] The corresponding structures of single-linker **spn** frameworks and **hxg** frameworks are obtained by removing one type of linker from the **sph** structures. Formates were used to replace the position of carboxylates in the removed linker.

AFM mechanical properties test

Topography images, elastic modulus, and indentation were acquired in AM-FM mode using an Oxford Instruments Asylum Research MFP-3D AFM equipped with the NanoMechPro tool option. The technique exploits a dual-resonance excitation allowing the real-time measurements of surface morphology, performed in AM

mode on the fundamental resonance of the cantilever, and mechanical properties were derived from FM mode using a higher overtone. For all the measurements, we used Asylum AC160TS-R2 silicon cantilevers with a nominal tip curvature radius of 8 nm and nominal spring constant of the fundamental harmonics (nominal resonance frequency: 300 kHz) of 42 $N \cdot m^{-1}$. Tip radius, oscillation amplitude, and cantilever spring constant were calibrated at each measurement, and measured values were used for Young's modulus computation. More detailed methods of AFM mechanical properties tests can be found in the supplemental information.

SUPPLEMENTAL INFORMATION

ACKNOWLEDGMENTS

AUTHOR CONTRIBUTIONS

Conceptualization, H.J. and M.E.; methodology, H.J., S.M.M., B.S., and M.E.; investigation, H.J., S.M.M., J.C.-J., B.T., A.S., Z.O.A., J.J., N.A., and O.S.; writing – original draft, H.J., S.M.M., and M.E.; writing – review & editing, H.J., S.M.M., J.C.-J., B.T., A.S., B.S., and M.E.; funding acquisition, E.D.F., B.S., and M.E.; supervision, M.E.

DECLARATION OF INTERESTS

The authors declare no competing interests.

REFERENCES

1. Furukawa, H., Cordova, K.E., O'Keeffe, M., and Yaghi, O.M. (2013). The chemistry and applications of metal-organic frameworks. Science *341*, 1230444. https://doi.org/10.1126/science.1230444.

2. Jiang, H., Alezi, D., and Eddaoudi, M. (2021). A reticular chemistry guide for the design of periodic solids. Nat. Rev. Mater. *6*, 466–487. https://doi.org/10.1038/s41578-021-00287-y.

3. Yaghi, O.M. (2016). Reticular chemistry—construction, properties, and precision reactions of frameworks. J. Am. Chem. Soc. *138*, 15507–15509. https://doi.org/10.1021/jacs.6b11821.

4. Alsadun, N., Mouchaham, G., Guillerm, V., Czaban-Jóźwiak, J., Shkurenko, A., Jiang, H., Bhatt, P.M., Parvatkar, P., and Eddaoudi, M. (2020). Introducing a cantellation strategy for the design of mesoporous zeolite-like metal–organic frameworks: Zr-sod-ZMOFs as a case study. J. Am. Chem. Soc. *142*, 20547–20553. https://doi.org/10.1021/jacs.0c10007.

5. Assen, A.H., Belmabkhout, Y., Adil, K., Bhatt, P.M., Xue, D.-X., Jiang, H., and Eddaoudi, M. (2015). Ultra-Tuning of the rare-earth fcu-MOF aperture size for selective molecular exclusion of branched paraffins. Angew. Chem. Int. Ed. Engl. *54*, 14353–14358. https://doi.org/10.1002/anie.201506345.

6. Xue, D.-X., Belmabkhout, Y., Shekhah, O., Jiang, H., Adil, K., Cairns, A.J., and Eddaoudi, M. (2015). Tunable rare earth fcu-MOF platform: access to adsorption kinetics driven gas/vapor separations via pore size contraction. J. Am. Chem. Soc. *137*, 5034–5040. https://doi.org/10.1021/ja5131403.

7. Bhatt, P.M., Belmabkhout, Y., Assen, A.H., Weseliński, Ł.J., Jiang, H., Cadiau, A., Xue, D.-X., and Eddaoudi, M. (2017). Isoreticular rare earth fcu-MOFs for the selective removal of H2S from CO2 containing gases. Chem. Eng. J. *324*, 392–396. https://doi.org/10.1016/j.cej.2017.05.008.

8. Xue, D.-X., Cadiau, A., Weseliński, Ł.J., Jiang, H., Bhatt, P.M., Shkurenko, A., Wojtas, L., Chen, Z., Belmabkhout, Y., Adil, K., and Eddaoudi, M. (2018). Topology meets MOF chemistry for pore-aperture fine tuning: ftw-MOF platform for energy-efficient separations via adsorption kinetics or molecular sieving. Chem. Commun.

54, 6404–6407. https://doi.org/10.1039/C8CC03841D.

9. He, T., Kong, X.-J., Bian, Z.-X., Zhang, Y.-Z., Si, G.-R., Xie, L.-H., Wu, X.-Q., Huang, H., Chang, Z., Bu, X.-H., et al. (2022). Trace removal of benzene vapour using double-walled metal–dipyrazolate frameworks. Nat. Mater. *21*, 689–695. https://doi.org/10.1038/s41563-022-01237-x.

10. Thiam, Z., Abou-Hamad, E., Dereli, B., Liu, L., Emwas, A.-H., Ahmad, R., Jiang, H., Isah, A.A., Ndiaye, P.B., Taoufik, M., et al. (2020). Extension of surface organometallic chemistry to metal–organic frameworks: development of a well-defined single site [(≡Zr–O–) W(O)(CH2tBu)3] olefin metathesis catalyst. J. Am. Chem. Soc. *142*, 16690–16703. https://doi.org/10.1021/jacs.0c06925.

11. Ma, L., Abney, C., and Lin, W. (2009). Enantioselective catalysis with homochiral metal-organic frameworks. Chem. Soc. Rev. *38*, 1248–1256. https://doi.org/10.1039/B807083K.

12. Mondloch, J.E., Katz, M.J., Isley, W.C., Iii, Ghosh, P., Liao, P., Bury, W., Wagner, G.W., Hall, M.G., DeCoste, J.B., Peterson, G.W., et al. (2015). Destruction of chemical warfare agents using metal–organic frameworks. Nat. Mater. *14*, 512–516. https://doi.org/10.1038/nmat4238.

13. Nam, D.-H., Shekhah, O., Lee, G., Mallick, A., Jiang, H., Li, F., Chen, B., Wicks, J., Eddaoudi, M., and Sargent, E.H. (2020). Intermediate binding control using metal–organic frameworks enhances electrochemical CO2 reduction. J. Am. Chem. Soc. *142*, 21513–21521. https://doi.org/10.1021/jacs.0c10774.

14. Kornienko, N., Zhao, Y., Kley, C.S., Zhu, C., Kim, D., Lin, S., Chang, C.J., Yaghi, O.M., and Yang, P. (2015). Metal–organic frameworks for electrocatalytic reduction of carbon dioxide. J. Am. Chem. Soc. *137*, 14129–14135. https://doi.org/10.1021/jacs.5b08212.

15. Li, M., Wan, Y., Huang, J.-K., Assen, A.H., Hsiung, C.-E., Jiang, H., Han, Y., Eddaoudi, M., Lai, Z., Ming, J., and Li, L.-J. (2017). Metal–organic framework-based separators for enhancing Li–S battery stability: mechanism of mitigating polysulfide diffusion. ACS Energy Lett. *2*, 2362–2367. https://doi.org/10.1021/acsenergylett.7b00692.

16. Howarth, A.J., Liu, Y., Li, P., Li, Z., Wang, T.C., Hupp, J.T., and Farha, O.K. (2016). Chemical, thermal and mechanical stabilities of metal–organic frameworks. Nat. Rev. Mater. *1*, 15018. https://doi.org/10.1038/natrevmats.2015.18.

17. Tan, J.C., and Cheetham, A.K. (2011). Mechanical properties of hybrid inorganic–organic framework materials: establishing fundamental structure–property relationships. Chem. Soc. Rev. *40*, 1059–1080. https://doi.org/10.1039/C0CS00163E.

18. Yuan, S., Feng, L., Wang, K., Pang, J., Bosch, M., Lollar, C., Sun, Y., Qin, J., Yang, X., Zhang, P., et al. (2018). Stable metal–organic frameworks: design, synthesis, and applications. Adv. Mater. *30*, 1704303. https://doi.org/10.1002/adma.201704303.

19. He, T., Kong, X.-J., and Li, J.-R. (2021). Chemically stable metal–organic frameworks: rational construction and application expansion. Acc. Chem. Res. *54*, 3083–3094. https://doi.org/10.1021/acs.accounts.1c00280.

20. Chapman, K.W., Halder, G.J., and Chupas, P.J. (2009). Pressure-induced amorphization and porosity modification in a Metal–Organic framework. J. Am. Chem. Soc. *131*, 17546–17547. https://doi.org/10.1021/ja908415z.

21. Redfern, L.R., and Farha, O.K. (2019). Mechanical properties of metal–organic frameworks. Chem. Sci. *10*, 10666–10679. https://doi.org/10.1039/C9SC04249K.

22. Moosavi, S.M., Boyd, P.G., Sarkisov, L., and Smit, B. (2018). Improving the mechanical stability of metal–organic frameworks using chemical caryatids. ACS Cent. Sci. *4*, 832–839. https://doi.org/10.1021/acscentsci.8b00157.

23. Moghadam, P.Z., Rogge, S.M., Li, A., Chow, C.-M., Wieme, J., Moharrami, N., Aragones-Anglada, M., Conduit, G., Gomez-Gualdron, D.A., Van Speybroeck, V., and Fairen-Jimenez, D. (2019). Structure-mechanical stability relations of metal-organic frameworks via machine learning. Matter *1*, 219–234. https://doi.org/10.1016/j.matt.2019.03.002.

24. Ortiz, A.U., Boutin, A., Fuchs, A.H., and Coudert, F.-X. (2012). Anisotropic elastic properties of flexible metal-organic frameworks: how soft are soft porous crystals? Phys. Rev. Lett. *109*, 195502. https://doi.org/10.1103/PhysRevLett.109.195502.

25. Bouëssel du Bourg, L., Ortiz, A.U., Boutin, A., and Coudert, F.-X. (2014). Thermal and mechanical stability of zeolitic imidazolate frameworks polymorphs. Apl. Mater. *2*, 124110. https://doi.org/10.1063/1.4904818.

26. Rogge, S.M.J., Waroquier, M., and Van Speybroeck, V. (2018). Reliably modeling the mechanical stability of rigid and flexible metal–organic frameworks. Acc. Chem. Res. *51*, 138–148. https://doi.org/10.1021/acs.accounts.7b00404.

27. Wu, H., Yildirim, T., and Zhou, W. (2013). Exceptional mechanical stability of highly porous zirconium metal–organic framework UiO-66 and its important implications. J. Phys. Chem. Lett. *4*, 925–930. https://doi.org/10.1021/jz4002345.

28. Tan, J.C., Bennett, T.D., and Cheetham, A.K. (2010). Chemical structure, network topology, and porosity effects on the mechanical properties of Zeolitic Imidazolate Frameworks. Proc. Natl. Acad. Sci. USA. *107*, 9938–9943. https://doi.org/10.1073/pnas.1003205107.

29. Henke, S., Li, W., and Cheetham, A.K. (2014). Guest-dependent mechanical anisotropy in pillared-layered soft porous crystals – a nanoindentation study. Chem. Sci. *5*, 2392–2397. https://doi.org/10.1039/C4SC00497C.

30. Zeng, Z., and Tan, J.-C. (2017). AFM nanoindentation to quantify mechanical properties of nano- and micron-sized crystals of a metal–organic framework material. ACS Appl. Mater. Interfaces *9*, 39839–39854. https://doi.org/10.1021/acsami.7b13402.

31. Kapustin, E.A., Lee, S., Alshammari, A.S., and Yaghi, O.M. (2017). Molecular retrofitting adapts a metal–organic framework to extreme pressure. ACS Cent. Sci. *3*, 662–667. https://doi.org/10.1021/acscentsci.7b00169.

32. Lal, G., Derakhshandeh, M., Akhtar, F., Spasyuk, D.M., Lin, J.-B., Trifkovic, M., and Shimizu, G.K.H. (2019). Mechanical properties of a metal–organic framework formed by covalent cross-linking of metal–organic polyhedra. J. Am. Chem. Soc. *141*, 1045–1053. https://doi.org/10.1021/jacs.8b11527.

33. Iizuka, T., Honjo, K., and Uemura, T. (2019). Enhanced mechanical properties of a metal–organic framework by polymer insertion. Chem. Commun. *55*, 691–694. https://doi.org/10.1039/C8CC08922A.

34. Ockwig, N.W., Delgado-Friedrichs, O., O'Keeffe, M., and Yaghi, O.M. (2005). Reticular chemistry: occurrence and taxonomy of nets and grammar for the design of frameworks. Acc. Chem. Res. *38*, 176–182. https://doi.org/10.1021/ar020022l.

35. Lyu, H., Ji, Z., Wuttke, S., and Yaghi, O.M. (2020). Digital reticular chemistry. Chem *6*, 2219–2241. https://doi.org/10.1016/j.chempr.2020.08.008.

36. Chen, Z., Jiang, H., O'Keeffe, M., and Eddaoudi, M. (2017). Minimal edge-transitive nets for the design and construction of metal–organic frameworks. Faraday Discuss *201*, 127–143. https://doi.org/10.1039/C7FD00119C.

37. Chen, Z., Weseliński, Ł.J., Adil, K., Belmabkhout, Y., Shkurenko, A., Jiang, H., Bhatt, P.M., Guillerm, V., Dauzon, E., Xue, D.-X., et al. (2017). Applying the power of reticular chemistry to finding the missing alb-MOF platform based on the (6, 12)-coordinated edge-transitive net. J. Am. Chem. Soc. *139*, 3265–3274. https://doi.org/10.1021/jacs.7b00219.

38. Jiang, H., Jia, J., Shkurenko, A., Chen, Z., Adil, K., Belmabkhout, Y., Weselinski, L.J., Assen, A.H., Xue, D.-X., O'Keeffe, M., and Eddaoudi, M. (2018). Enriching the reticular chemistry repertoire: merged nets approach for the rational design of intricate mixed-linker metal–organic framework platforms. J. Am. Chem. Soc. *140*, 8858–8867. https://doi.org/10.1021/jacs.8b04745.

39. Chen, Z., Jiang, H., Li, M., O'Keeffe, M., and Eddaoudi, M. (2020). Reticular chemistry 3.2: typical minimal edge-transitive derived and related nets for the design and synthesis of metal–organic frameworks. Chem. Rev. *120*, 8039–8065. https://doi.org/10.1021/acs.chemrev.9b00648.

40. Mayo, S.L., Olafson, B.D., and Goddard, W.A. (1990). DREIDING: a generic force field for molecular simulations. J. Phys. Chem. *94*, 8897–8909. https://doi.org/10.1021/j100389a010.

41. Boyd, P.G., Moosavi, S.M., Witman, M., and Smit, B. (2017). Force-field prediction of materials properties in metal-organic frameworks. J. Phys. Chem. Lett. *8*, 357–363. https://doi.org/10.1021/acs.jpclett.6b02532.

42. Thompson, A.P., Aktulga, H.M., Berger, R., Bolintineanu, D.S., Brown, W.M., Crozier, P.S., in 't Veld, P.J., Kohlmeyer, A., Moore, S.G., Nguyen, T.D., et al. (2022). Lammps - a flexible simulation tool for particle-based materials modeling at the atomic, meso, and continuum scales. Comput. Phys. Commun. *271*, 108171. https://doi.org/10.1016/j.cpc.2021.108171.